High-angle wave instability and emergent shoreline shapes: 1. Modeling of sand waves, flying spits, and capes

Andrew D. Ashton[1,2] and A. Brad Murray[1]

[1] Contrary to traditional findings, the deepwater angle of wave approach strongly affects plan view coastal evolution, giving rise to an antidiffusional "high wave angle" instability for sufficiently oblique deepwater waves (with angles between wave crests and the shoreline trend larger than the value that maximizes alongshore sediment transport, ~45°). A one-contour-line numerical model shows that a predominance of high-angle waves can cause a shoreline to self-organize into regular, quasiperiodic shapes similar to those found along many natural coasts at scales ranging from kilometers to hundreds of kilometers. The numerical model has been updated from a previous version to include a formulation for the widening of an overly thin barrier by the process of barrier overwash, which is assumed to maintain a minimum barrier width. Systematic analysis shows that the wave climate determines the form of coastal response. For nearly symmetric wave climates (small net alongshore sediment transport), cuspate coasts develop that exhibit increasing relative cross-shore amplitude and pointier tips as the proportion of high-angle waves is increased. For asymmetrical wave climates, shoreline features migrate in the downdrift direction, either as subtle alongshore sand waves or as offshore-extending "flying spits," depending on the proportion of high-angle waves. Numerical analyses further show that the rate that the alongshore scale of model features increases through merging follows a diffusional temporal scale over several orders of magnitude, a rate that is insensitive to the proportion of high-angle waves. The proportion of high-angle waves determines the offshore versus alongshore aspect ratio of self-organized shoreline undulations.

Citation: Ashton, A. D., and A. B. Murray (2006), High-angle wave instability and emergent shoreline shapes: 1. Modeling of sand waves, flying spits, and capes, *J. Geophys. Res.*, *111*, F04011, doi:10.1029/2005JF000422.

1. Introduction

1.1. Overview

[2] Although the shoreline is perhaps the most dynamic geologic boundary on the Earth's surface, minor changes in its position can have major economic and societal consequences. Along a coast composed of mobile, noncohesive sediment, relatively small gradients in alongshore sediment transport can locally overwhelm changes in shoreline position due to sea level fluctuations [*Cowell et al.*, 1995], particularly when the planform of the coast curves. Previous studies predict that alongshore sediment transport will tend to smooth undulations along an otherwise straight sandy shoreline, as described by a diffusion equation [*Pelnard-Considéré*, 1956; *Larson et al.*, 1987]. However, *Ashton et al.* [2001] demonstrated that a sandy shoreline is unstable when the angle between deepwater wave crests and the shoreline trend ("wave angle") is large. Shoreline instability merely requires a maximum in alongshore sediment transport for a given wave angle (Figure 1). Waves approaching a shoreline at angles greater than this maximizing angle ("high-angle" waves) can cause a coast to self-organize into quasiperiodic, large-scale shoreline features such as alongshore sand waves and cuspate spits [*Ashton et al.*, 2001].

[3] This paper further explores the consequences of the instability presented by *Ashton et al.* [2001]. Section two examines analytical predictions of shoreline evolution and stability, including predictions of the finite amplitude evolution of a single bump subjected to high-angle waves approaching from a fixed direction. The numerical model of shoreline change, with the addition of a barrier overwash algorithm, is described in detail in section three. Next, we present the numerical model results, including a phase diagram showing how the appearance of distinctly different morphological features depends on wave climate characteristics. We also analyze how different wave climates affect large-scale features' aspect ratios and rates of wavelength growth. This paper concludes with a discussion of the predictions made by the numerical model and model limitations. In a companion paper [*Ashton and Murray*, 2006],

[1]Division of Earth and Ocean Sciences, Nicholas School of the Environment and Earth Sciences and Center for Nonlinear and Complex Systems, Duke University, Durham, North Carolina, USA.
[2]Now at Department of Geology and Geophysics, Woods Hole Oceanographic Institution, Woods Hole, Massachusetts, USA.
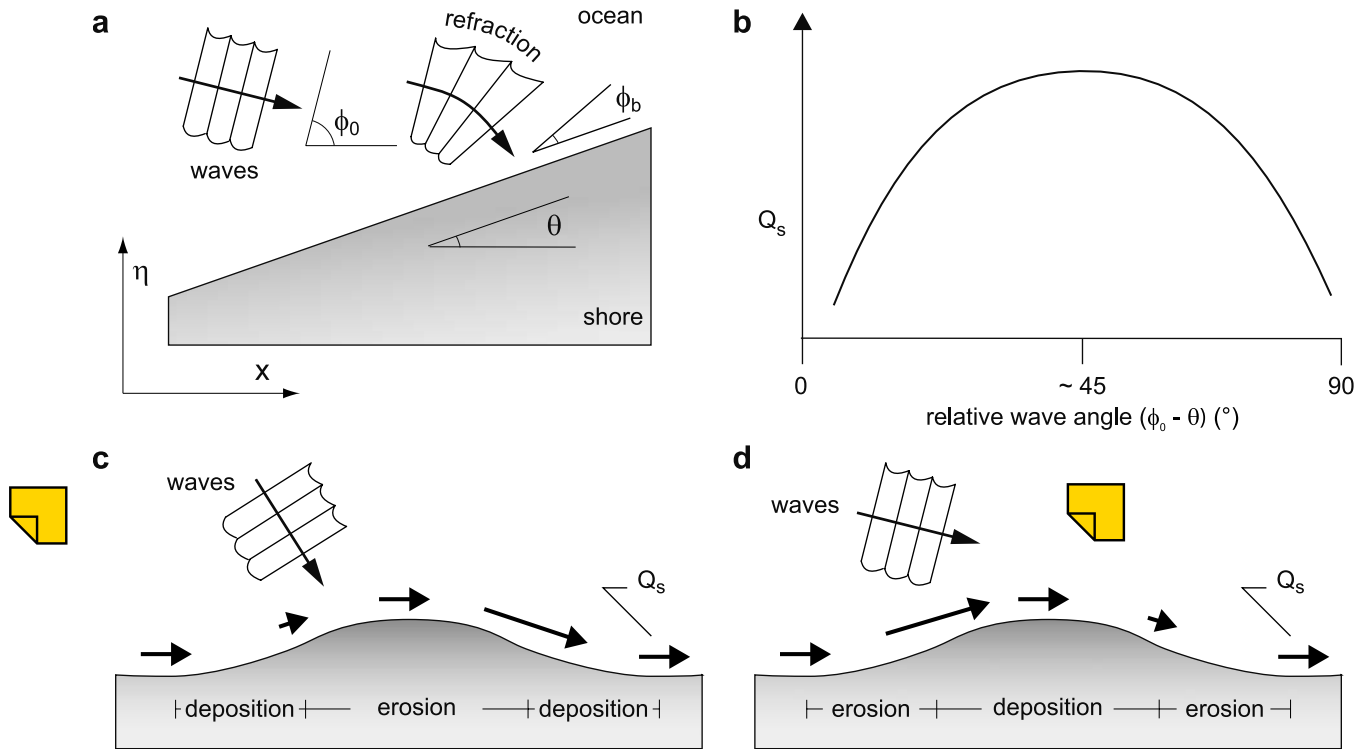
Figure 1. Illustrations depicting the high wave angle instability in shoreline shape. (a) Depiction of terms and axes. (b) Schematic of the relationship between alongshore sediment transport (Q_s) and relative wave angle ($\phi_0 - \theta$), showing a maximum in Q_s for ($\phi_0 - \theta$) $\approx 45°$. (c) Response of a perturbation to a plan view shoreline subjected to low-angle waves (($\phi_0 - \theta$) $< \sim45°$). Sediment flux increases downdrift along the flanks and increases along the crest, resulting in flattening of the shape. (d) Opposite response for high-angle waves, with erosion along the flanks where ($\phi_0 - \theta$) is decreasing (Q_s diverging) and accretion along the crest as ($\phi_0 - \theta$) increases (Q_s converging).

we present techniques for studying wave climates, and then apply these techniques to natural and simulated coasts in an effort to further test the model predictions and the hypothesis that high-angle waves are responsible for the evolution and maintenance of several classes of large-scale shoreline features.

1.2. Background

[4] Rhythmic shoreline features appear across a wide range of scales [*Dolan and Ferm*, 1968; *Komar*, 1998], from swash zone beach cusps, crescentic bars [*Wright and Short*, 1984], rip-related megacusps [*Komar*, 1983], up to cuspate forelands [*Hoyt and Henry*, 1971]. Although infragravity edge waves have historically been associated with regular, periodic coastal features, more recent research focusing not only on hydrodynamics, but also on sediment transport feedbacks suggest that instabilities, nonlinearity, and self-organization play a strong role in the formation of features such as beach cusps [*Werner and Fink*, 1993; *Coco et al.*, 2000] and rhythmic nearshore bars [*Deigaard et al.*, 1999; *Falqués et al.*, 2000]. However, less quantitative attention has been paid to the formation of rhythmic features with alongshore spatial scales significantly larger than that of the surf zone.

[5] Although *Dolan et al.* [1979] suggested that edge waves may be important at much larger scales (several tens of kilometers), others hypothesize that the periodicity of large-scale shoreline features may arise from preexisting geologic templates (perhaps inherited from river valley geometry [*Hoyt and Henry*, 1971]), or, at smaller scales, periodicities in sediment inputs [*Thevenot and Kraus*, 1995] or bar merging [*Davidson-Arnott and Van Heyningen*, 2003]. In a qualitative manner, *Zenkovich* [1959, 1967] noted not only that a maximizing angle for sediment transport may control the formation of cuspate spits, but that smaller spits could be "annihilated" by larger ones. The hypothesis that an instability in shoreline shape controls both the generation and maintenance of large-scale rhythmic features discussed here differs significantly from edge wave or geologic inheritance hypotheses in that not only do series of large-scale cuspate forelands and spits remain dynamic landforms, but that their spatial scales change over the course of their evolution. This self-organizing behavior follows directly from the presence of a maximizing angle for alongshore sediment transport.

2. Alongshore Sediment Transport and the High Wave Angle Instability

2.1. Alongshore Sediment Transport

[6] Various expressions relate wave-breaking-induced alongshore sediment transport to its driving forces, such as wave height and angle. The most common of these relationships, sometimes referred to as either the CERC
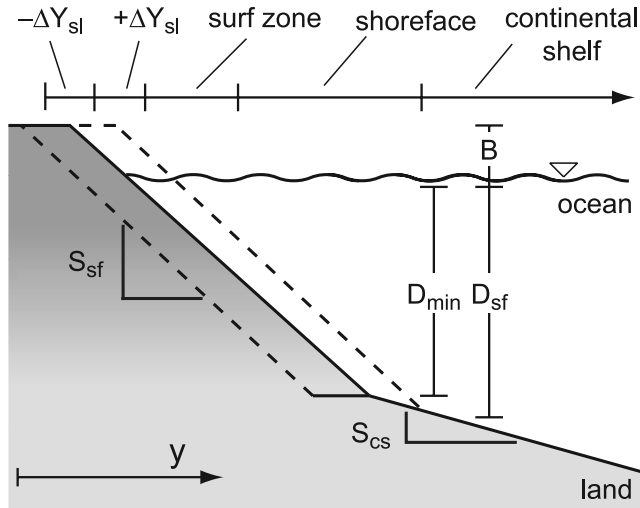
Figure 2. Cross-shore schematization (with extreme vertical exaggeration) demonstrating the conservation of nearshore sediment. Although alongshore sediment transport and its gradients are concentrated close to the shore in the surf zone, these losses or gains are spread over the effective shoreface depth. In this example, accretion ($+\Delta Y$) occurs up to a depth defined by the intersection of the shoreface with the continental shelf (D_{sf}), whereas erosion ($-\Delta Y$) maintains a minimum shoreface depth (D_{min}).

[Rosati et al., 2002] or Komar [1971] formula, relates volumetric alongshore sediment transport (Q_s, m³/day) to the breaking wave height (H_b, m) and wave angle:

$$Q_s = K_1 H_b^{\frac{5}{2}} \cos(\phi_b - \theta) \sin(\phi_b - \theta), \quad (1)$$

where ϕ_b is the breaking wave crest angle and θ is the shoreline orientation (Figure 1a). The empirical constant K_1, which relates the driving forces to volumetric sediment flux, typically equals ~0.4 m¹ᐟ²/s for quartz density sand [Komar, 1998; Rosati et al., 2002].

2.2. Traditional Predictions of Shoreline Evolution

[7] Traditional approaches to predicting large-scale shoreline evolution assume that sediment accumulations or deficits in the surf zone are spread evenly across the shoreface down to a depth, D_{sf}, below which cross-shore fluxes are negligible compared to the gradients in alongshore fluxes above this depth (Figure 2) [Komar, 1973; Larson et al., 1987; Hanson and Kraus, 1989]. This assumption allows coastal evolution to be tracked following only a single contour line, such as the shoreline location itself; correspondingly, this approach has been termed the "one-contour-line" or "one-line" technique.

[8] If nearshore sediment is conserved,

$$\frac{d\eta}{dt} = -\frac{1}{D_{sf}} \frac{dQ_s}{dx}, \quad (2)$$

where η is the position of the shoreline and t is time (Figure 1a). Traditional analytical one-line investigations further assume that ϕ_b and H_b are constant along an

undulating shoreline. Combining (1) with (2), and assuming small breaking wave angles ($\sin(\phi_b - \theta) \approx \tan(\phi_b - \theta) \approx d\eta/dx$), yields a formula for the time evolution of a shoreline:

$$\frac{d\eta}{dt} = -\frac{K_1}{D_{sf}} H_b^{\frac{5}{2}} \frac{d^2\eta}{dx^2}, \quad (3)$$

a diffusion equation for shoreline change similar to the one first presented by Pelnard-Considéré [1956]. This expression, predicting that all perturbations to a straight coast will flatten over time at a rate independent of wave angle, has been in use for almost five decades [Pelnard-Considéré, 1956, 1984; Larson et al., 1987, 1997; Rosati et al., 2002]. Wang and LeMehaute [1980] warned that if the small breaking angle assumption did not hold, (3) could lead to an unstable shoreline for breaking wave angles greater than ~45°. However, as waves breaking at such large angles are unlikely, they concluded that the breaking angle instability is more likely to occur in numerical models than along natural coasts.

[9] However, wave refraction, the same phenomenon that results in small breaking wave angles, causes H_b to vary significantly along a sinuous shoreline. As we demonstrate below, for most wave approach angles, the classical diffusion, or Pelnard-Considéré, solution is inappropriate, and, despite its common application, (3) does not generally apply to shoreline evolution.

2.3. Angle-Dependant Shoreline Diffusivity and the Instability in Shoreline Shape

[10] As waves approach shore, they shoal (enter decreasing water depth), typically reducing their speed (celerity) and increasing their heights. Waves approaching a coast at an angle also refract as they shoal, with their crests becoming more shore-parallel. This refraction, in turn, reduces wave heights as wave crests are stretched. As a result, breaking wave angle and breaking wave height are interdependent, a phenomenon that is particularly pronounced when waves approach with large deepwater angles. H_b cannot be considered constant along an undulating coast (Figure 3) [Ashton et al., 2001].

[11] Therefore (3) should be replaced with either a function that accounts for predicted changes in H_b due to refraction or with a function that is in terms of globally constant variables. The deepwater wave quantities, ϕ_0 and H_0, unaffected by shoaling and refraction, can be considered constant along a coast. Assuming refraction over shore-parallel contours, breaking waves are fully shallow water waves, wave breaking is depth-limited, and

$$\cos^{\frac{1}{5}}(\phi_b - \theta) \approx 1 \quad (4)$$

(1) can be transformed to a deepwater formula:

$$Q_s = K_2 H_0^{\frac{12}{5}} T^{\frac{1}{5}} \cos^{\frac{6}{5}}(\phi_0 - \theta) \sin(\phi_0 - \theta). \quad (5)$$

The ratio of K_2 to K_1 is constant:

$$K_2 = \left(\frac{\sqrt{g\gamma}}{2\pi}\right)^{\frac{1}{5}} K_1, \quad (6)$$
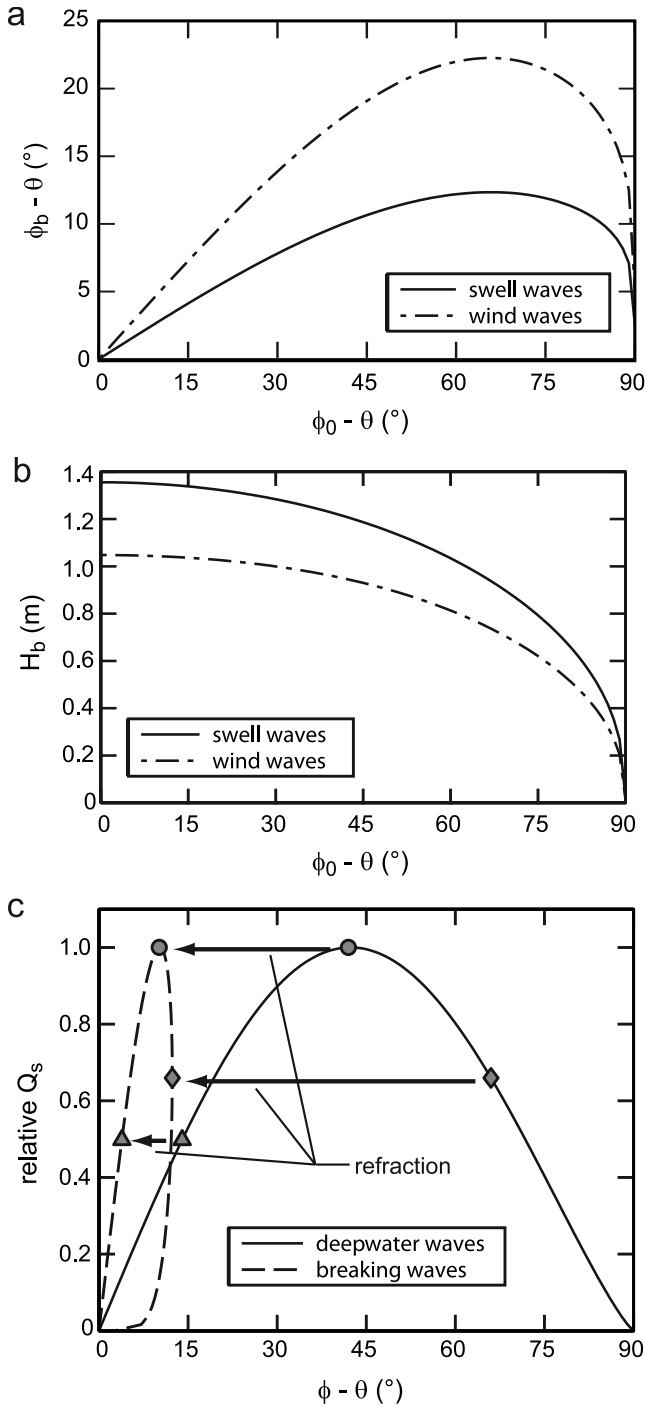
Figure 3. Breaking wave quantities (a) $(\phi_b - \theta)$ and (b) H_b for waves refracted over shore-parallel contours using linear wave theory and assuming depth-limited breaking, as a function of $(\phi_0 - \theta)$, for representative wind (dash-dotted line, $H_0 = 2$ m $T = 7$ s) and swell (solid line, $H_0 = 2$ m $T = 15$ s) waves. Note that with higher-angle waves, $(\phi_b - \theta)$ becomes relatively constant, while H_b varies considerably as $(\phi_0 - \theta)$ is varied. (c) Resultant alongshore sediment transport (Q_s) for swell waves in terms of deepwater $((\phi_0 - \theta)$, solid line) and breaking $((\phi_b - \theta)$, dashed line) angles. The depiction of the relationships in Figures 3a and 3b follow that of *Falqués* [2003].

where g is the acceleration of gravity and γ is the ratio of wave height to water depth for breaking waves [*Komar, 1998*]. Equation (5), which resembles a relationship derived independently by *Walton and Dean* [1973; *Dean and Dalrymple*, 2002], predicts a maximum in Q_s for deepwater waves approaching at relative angles of approximately 42° (Figure 3c).

[12] The similarity between (1) and (5) can be better understood by observing that the alongshore component of the radiation stress (S_{xy}, which drives the alongshore current), is conserved during refraction over shore-parallel contours [*Longuet-Higgins*, 1972], such that the relationship:

$$S_{xy} = H^2 \sin(\phi - \theta) \cos(\phi - \theta), \qquad (7)$$

remains appropriate for breaking, intermediate, and deep-water waves [*Longuet-Higgins*, 1970]. The remaining differences between (1) and (5) arise from the conversion of $H_b^{\frac{1}{2}}$ to deepwater quantities.

[13] Because of their similar form, equations (1) and (5) appear to be contradictory, predicting that Q_s is maximized for both breaking and deepwater waves at angles of approximately 45°. However, the 45° maximum in (1) assumes that H_b is constant, whereas in nature differing amounts of refraction result in an H_b that varies along an undulating coast (Table 1 and Figure 3) [*Ashton et al.*, 2001]. Holding H_b constant along a shoreline with a varying orientation (θ) would require specific alongshore adjustments to both H_0 and ϕ_0, a scenario that could not arise in nature. On the other hand, (5) predicts that along a natural shoreline affected by deepwater waves approaching from a fixed direction with a given height, shore-parallel refraction causes breaking wave heights and angles for a given deepwater wave to change concomitantly alongshore such that the actual maximum in Q_s occurs when the relative deepwater wave angle is approximately 42°, even if breaking angles will be much smaller than this maximizing angle (Table 1 and Figure 3). Although their details may differ, other formulations for Q_s show a similar maximum for a deepwater angle of about 45° [*Ashton and Murray*, 2006].

Table 1. Sample Calculated Breaking Wave Angles $(\phi_b - \theta)$ and Heights (H_b) and Subsequent Relative Alongshore Sediment Transport $(Q_s/\max(Q_s))$[a]

$(\phi_0 - \theta)$, deg	H_b, m	$(\phi_b - \theta)$, deg	$Q_s/\max(Q_s)$
0	2.38	0.0	0.0
15	2.35	5.5	0.53
30	2.26	10.4	0.90
45	2.09	14.2	1.00
60	1.82	16.3	0.80
75	1.40	15.9	0.40
89	0.47	9.4	0.02

[a]Calculated using (1) for swell waves with a deepwater wave height (H_0) of 2 m and period (T) of 10 s for different deepwater relative angles $(\phi_0 - \theta)$, assuming refraction over shore-parallel contours and depth-limited breaking [see *Komar*, 1998]. Note that the maximum alongshore sediment transport occurs when waves break at ~14°.
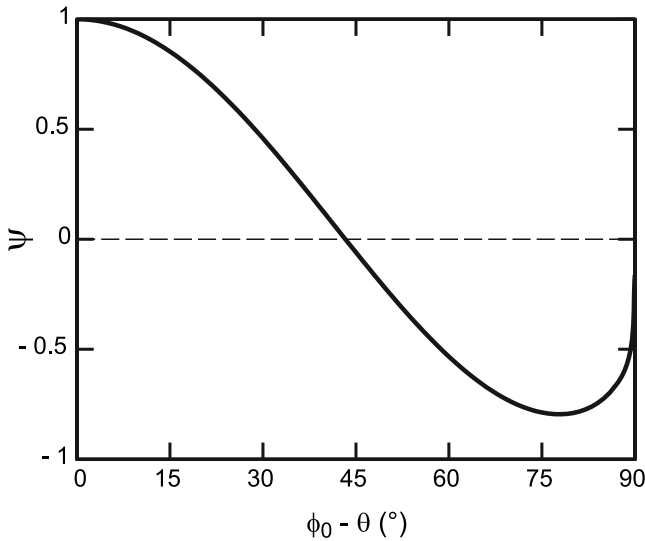
Figure 4. ψ, the angle dependence of the shoreline diffusivity, versus deepwater wave angle $(\phi_0 - \theta)$. Similar figures have been previously presented by *Murray and Ashton* [2003], *Ashton and Murray* [2003], and *Falqués* [2003].

2.4. Shoreline Instability

[14] Combining (2), the conservation of nearshore sediment, with the deepwater relationship for alongshore sediment transport, (5), and utilizing the chain rule yields:

$$\frac{d\eta}{dt} = -\frac{K_2}{D} H_0^{\frac{12}{5}} T^{\frac{1}{5}} \left\{ \cos^{\frac{1}{5}}(\phi_0 - \theta) \left[\cos^2(\phi_0 - \theta) \right. \right.$$
$$\left. \left. - \left(\frac{6}{5}\right) \sin^2(\phi_0 - \theta) \right] \right\} \frac{d^2\eta}{dx^2}, \tag{8}$$

a diffusion equation where the diffusivity has a wave angle dependence, ψ, equal to the term in the curly brackets (Figure 4) [*Murray and Ashton*, 2004]. Shoreline diffusivity decreases from a maximum for waves approaching directly onshore, passes through zero at the angle maximizing Q_s, and becomes negative for even more oblique wave angles (Figures 1c, 1d, and 4). This new shoreline evolution equation, as opposed to the Pelnard-Considéré formulation, accounts for all of the changes to wave properties due to simple wave refraction over shore-parallel contours.

[15] Even if all of the waves affecting a shoreline approach from low deepwater angles (with a nearly shore-normal approach such that refraction can be neglected and $\psi \sim 1$), after accounting for the difference between K_1 and K_2, the diffusivity predicted by (8) will be different than that predicted by (3). This overprediction of diffusivity by (3) arises because the actual diffusivity from (8) depends on deepwater, not breaking heights. Overprediction will be particularly pronounced for long-period swell waves that significantly increase their heights as they shoal. This could explain the apparent strong period dependence of the diffusivity suggested by *Falqués* [2003]. As shown by (8), the actual diffusivity only weakly depends upon wave period; the period dependence described by Falqués strictly pertains to the overprediction of shoreline diffusivity by previous methods.

[16] The presence of an instability in shoreline shape due to high-angle waves has been suggested previously. *Zenkovich* [1959, 1967], studying shoreline features in elongated water bodies, was perhaps the first to identify that a maximum in alongshore sediment transport can lead to an unstable shoreline. He qualitatively suggested that alongshore sediment transport is maximized for a wave angle of 45°. Also not specifying whether he was referring to breaking or deepwater waves, *Grijm* [1960, 1964] explored the shoreline shapes that could result from waves approaching from any one angle greater or less than a suggested maximizing transport angle of 45°. *Bakker* [1968] identified the potential for a high-angle instability, but much like *Wang and LeMehaute* [1980], studied the instability in terms of breaking wave quantities, and dismisses the possibility of the instability happening along a natural coast. In a novel approach, *Walton and Dean* [1973], studying the effects of integrated wave climates, predicted shoreline instability at zero-flux ("nodal") shoreline locations for certain types of wave climates. As explained by *Ashton and Murray* [2006], Walton and Dean's wave climate instability reduces to the case discussed here for a single wave approach angle.

2.5. Shoreline Perturbations Growing to Finite Amplitude

[17] Conceptually, the finite evolution of a single bump on a straight shoreline influenced by waves approaching from a single direction can be generally understood using the relationship shown in Figure 4. When waves approach from a fixed direction that is low angle along the entire shoreline, a subtle plan view bump will flatten with constant diffusivity. The angle-dependent diffusivity means that the traditional approach may overestimate the diffusivity constant if breaking wave quantities, as in (3), are used instead of deepwater quantities, as in (8).

[18] More importantly, if this bump is not subtle (of finite rather than infinitesimal amplitude), this flattening will diverge from classical diffusion because of the angle dependence; in general there will be a faster rate of change along the flanks and the top where the relative angles are smallest (Figure 4). Regardless, if wave angles remain low along an entire protuberance, it will soon flatten, even if the shape does not evolve as predicted by a linear diffusion equation (such as (3)).

[19] For the case where the entire coast is affected by waves from a single high-angle direction, a bump will initially accrete along its crest and erode along its flanks (Figure 5, time 1). The shoreline angle at the inflection point will increase, but cannot exceed the one that maximizes alongshore sediment transport (Figure 5, times 2 and 3). However, continued erosion along the updrift flank will tend to increase the angle at the inflection point, eventually forcing the inflection point to migrate toward the crest of the protuberance (Figure 5, time 4). The updrift flank will tend toward a constant erosion rate shoreline that approaches, but does not exceed the angle that maximizes sediment transport.

[20] Finite amplitude effects will also influence the downdrift evolution of this growing feature. As the crest accretes, the relative wave angle at the downdrift inflection point will approach a right angle, a zero-flux orientation (Figure 5,
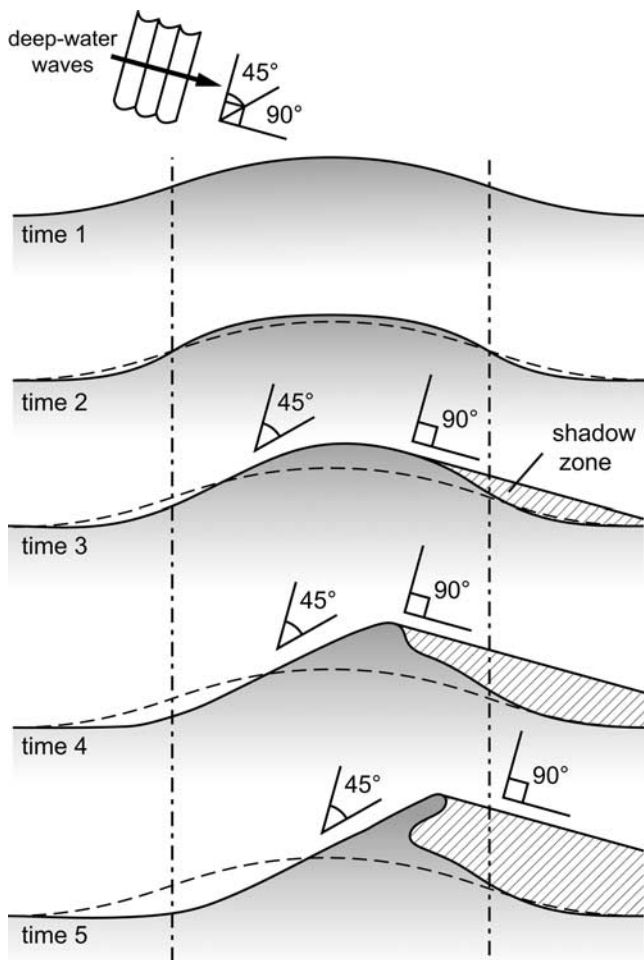
analyses, however, become increasingly irrelevant, as natural shorelines will be affected by an entire "climate" of waves approaching from different angles over time, and eventually the boundary conditions (particularly at the upstream end) could exert an influence over the evolution of growing features. More complicated finite amplitude behavior, such as the response of a coast to time-varying wave approach angles and the interaction of multiple finite-amplitude features along an extended spatial domain can more easily be studied using a numerical model.

3. Numerical Model

[23] To further explore shoreline evolution, we have created a numerical model, a version of which is briefly described by *Ashton et al.* [2001], with additional detail by *Murray and Ashton* [2004]. The updated version of the model described here in detail contains an algorithm for barrier overwash allowing a barrier to maintain a minimum width.

[24] Our modeling goal is not to simulate any one location in fine detail, but to study the types of shoreline behavior that can arise from the basic instability in shoreline shape. Extending the concepts of other common one-line models used in many coastal studies [*LeMehaute and Soldate*, 1977; *Ozasa and Brampton*, 1980; *Hanson and Kraus*, 1989], this model contains a new, numerically stable solution scheme to treat the case of high-angle waves. As suggested by the simple analysis above, the high-angle instability should lead to offshore-extending spits which present unique challenges to a line-based model; our model accommodates a shoreline that becomes arbitrarily sinuous, even doubling back on itself.

3.1. Model Setup
3.1.1. Model Domain
[25] The model domain represents a plan view with positions defined using globally alongshore (x direction) and cross-shore (y direction) coordinates. The domain is discretized into bins, or "cells", of a set width, ΔW (Figure 6). Each cell contains a value, F, representing the cell's fractional plan view area that is occupied by land. A cell with a value $F = 1$ represents dry land (a "land cell"); a cell with $F = 0$ is fully subaqueous (an "ocean cell"). The shoreline consists of the line of cells between land cells and ocean cells with $0 < F < 1$ (Figure 6).

[26] Because local shoreline orientations can diverge greatly from the global coastal orientation (the x direction), the fractional values within shoreline cells must be interpreted to determine the location of the coast at each time step. Typically, the fractional value within a cell represents the cross-shore extension of the subaerial shore (Figure 6). However, if there is no land cell behind (globally landward, or in the negative y direction) a partially full cell, the model then assumes that the shore extends in the x direction from a land cell to the left or the right (Figure 6). If no land cell exists either behind or on either side, the beach is underneath a spit and the shore extends in the negative y direction.
3.1.2. Model Iteration
[27] The model iteratively evolves the shoreline position using (1) and (2) for given deepwater wave conditions by

Figure 5. Expected finite amplitude temporal evolution of a sinusoidal plan view shoreline protuberance affected by waves approaching from a constant high angle. As the shoreline angle at the updrift flank of the feature increases, its relative angle approaches but cannot exceed the one which maximizes Q_s (~45°), eventually leading to downdrift migration of the inflection point. Establishment of a zero-flux point along the downdrift flank results in spit extension and establishment of a zone shadowed from direct wave approach.

time 3). The shape will extend offshore (Figure 5, times 4 and 5), accreting at a rate determined by the local gross downdrift alongshore sediment flux (as opposed to the other parts of the shape controlled by flux gradients).

[21] This accretion along the downdrift end and erosion along the updrift flank dictates that a shape will translate downdrift while growing. The updrift flank should approach an angle approximately 45° to the wave approach angle (not 45° to the shoreline trend as suggested by *Zenkovich* [1959, 1967]). Note that Figure 5 shows the hypothesized evolution of a shape influenced by an extremely high-angle wave. For less oblique high-angle waves, a growing bump will be more subtle.

[22] Other scenarios, for instance adding a finite amplitude perturbation to a smooth shoreline near the maximizing angle, can lead to other interesting modes of behavior. Such
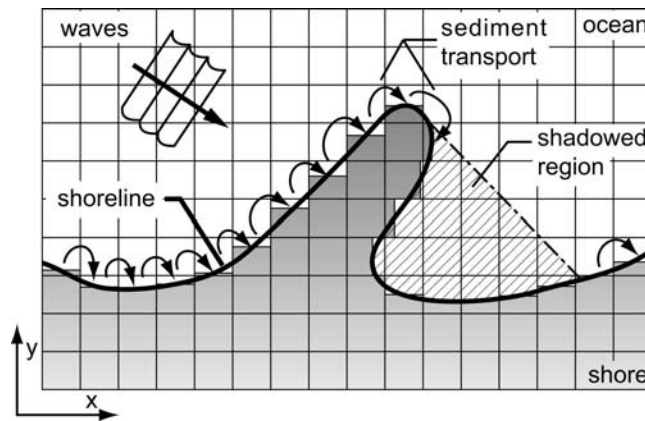
Figure 6. Plan view schematic of the model domain, demonstrating the interpreted shoreline configuration, the directions of sediment fluxes for a given wave approach angle, and the region shadowed from incoming waves.

bringing waves onshore assuming refraction over shore-parallel contours. During each iteration, the model interprets the shoreline configuration, determining alongshore sediment transport quantities, and updates the domain based upon gradients in the alongshore flux and the conservation of mass. As the shoreline extends seaward, it can "shadow" other portions of the shoreline from oncoming waves (Figure 6). Despite some of the complexity of the algorithm described below, in the straightforward case of a fairly straight coast subparallel to the x direction, our model simply discretizes (1) and (2), similar to other one-line models.

3.1.3. Underlying Assumptions

[28] We have created this model to specifically simulate shoreline evolution over long timescales (years and longer). Building upon the large-scale coastal behavior (LSCB) concept [*de Vriend et al.*, 1993], the model assumes that on larger spatial and temporal scales, gradients in alongshore sediment transport drive shoreline evolution. This approach assumes that smaller-scale behaviors, such as rip circulation and cusp formation, are superimposed upon general shoreline evolution trends, and that the shoreface profile retains a constant shape (Figure 2). An extension of the one-line approach, the model implicitly averages over short-term cross-shore redistribution of sediment, and does not resolve shoreline change on small timescales such as single storm events [*List and Farris*, 1999].

[29] This model can best be described as an "exploratory model", developed to increase our understanding of the key processes that affect shoreline evolution [*Murray*, 2003]. Underlying model assumptions prescribe a spatial scale below which the results should not be compared to nature. A simple wave refraction treatment assumes shore-parallel contours, neglecting the convergence and divergence of wave rays at headlands and embayments, respectively. These simplifications are reasonable for shoreline undulations with alongshore scales that are greater than the cross-shore extent of the shoreface. The shore-parallel assumption implicitly neglects how refraction over non-shore-parallel contours of the continental shelf (i.e., from the shelf break up to D_{sf}) may result in along-coast changes in wave angle and height (compared to the variations predicted by Snell's law for shore-parallel contours), a phenomenon that could

become more important as shoreline features extend farther across the shelf. Although evaluating the incoming wave angles at an intermediate-depth reference frame (set at D_{sf}) will account for this nonparallel refraction, wave heights cannot be assumed to be alongshore uniform if wave transformation has occurred over alongshore varying bathymetry.

3.2. Model Algorithm Details
3.2.1. Avoiding Discretization Errors

[30] The model algorithm utilizes two different shoreline orientations, a boundary-based angle computed between two adjacent cells and a cell-based angle computed between a cell's left and right neighbors (Figure 7). Often, one-line models will perform sediment transport calculations using a central differencing scheme, where the boundary-based angle between adjacent cells determines sediment transport. However, high-angle waves cause such a numerical solution scheme to become unstable [*Wang and LeMehaute*, 1980]. Moving along an otherwise straight shoreline, high-angle waves cause erosion upon reaching the beginning of a bump. Central differencing makes this erosion occur on the cell updrift of the beginning of the bump, resulting in an updrift migrating "erosion wave" that is entirely a discretization artifact [*Murray and Ashton*, 2004]. Therefore, for high-angle waves, we use an upwind differencing scheme (which determines the sediment transport using the angle across the previous cell boundary in the updrift direction); for locally low-angle waves, we use a central differencing scheme (Figure 7).

[31] Although the blend of central and upwind differencing resolves one discretization problem, it can lead to another discretization artifact. Passing downdrift from low- to high-angle shoreline segments, the same angle would be used to determine sediment transport across both the upstream and downstream boundaries of the transition cell, artificially preventing shoreline change at this location. Moving between low- and high-angle shoreline cells means that some part of a continuous shore will be at an angle that maximizes alongshore sediment transport. Accordingly, in our discretized case, the flux-maximizing angle determines sediment transport across the downdrift boundary of this transition cell (where upwind differencing would be used
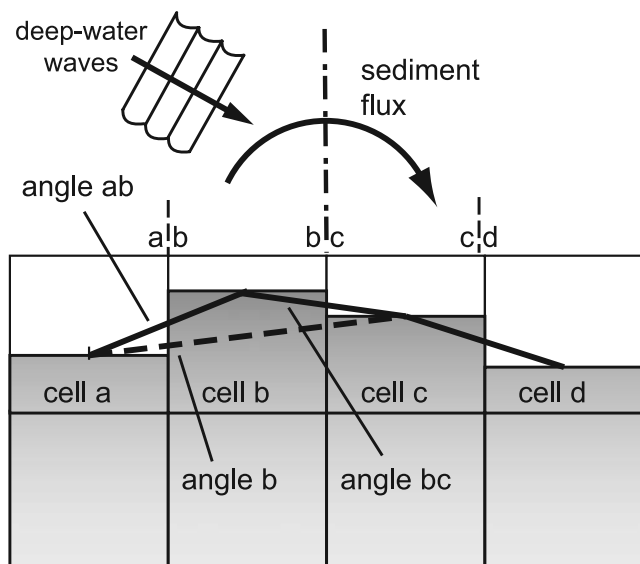
Figure 7. Plan view schematic of the numerical model solution scheme implemented for flux across a selected boundary *bc*. The local boundary-based angle across the boundary in question (angle *bc*) and the wave approach angle determine the sediment transport direction. The cell-based angle for the cell that sediment is transported from determines the differencing technique used; a central difference scheme is applied for low-angle waves, and an upwind scheme is applied for high-angle waves. In this example, the boundary-based angle *bc* predicts transport to the right from cell *b* to cell *c* for the shown wave approach direction. If the angle between the wave crests and the cell-based slope at *b* is greater than 42°, the upwind scheme is used; flux across boundary *bc* is computed using a transport angle equal to angle *ab*. Otherwise, for low-angle waves, sediment transport calculations use angle *bc* as the transport angle.

otherwise). The maximum flux is also enforced in the complimentary case of passing from high to low angles. Enforcement of the maximum in sediment transport actually has small effects on model evolution because gradients in Q_s (and therefore rates of shoreline change) are small when the coastal orientation approaches the flux-maximizing angle (Figure 4).

3.2.2. Wave Shadowing

[32] As shoreline protuberances extend seaward, they can shadow other portions of the shoreline from oncoming waves (Figure 6). At each cell, a linear search in the direction waves are approaching from determines if other portions of the shore will block approaching waves. If another portion of the shore interferes with a cell's line of sight, it shadows the cell from the dominant waves. This simplified linear search neglects the effects of the relatively small amounts of wave energy that could refract or diffract into shadowed regions. As one of the underlying model assumptions holds that protuberances are large compared to the shoreface, wave refraction should occur close to the shore and this effect will be minimal. This approach also means that the model neglects the possibility for wind generation of waves within a shadowed region.

[33] Shadowing can affect the selection of upwind and downwind solution schemes. The algorithm avoids using shoreline information from within shadowed regions to determine sediment fluxes. Transport into shadowed cells uses the upwind differencing scheme. Moving out of a shadowed region, the central differencing scheme therefore determines sediment transport between the first two unshadowed cells. For high-angle waves, no sediment is transported between the first two cells downdrift of the shadowed region. Otherwise, the second cell updrift of the shadowed region would have the same influx and outflux, artificially preventing shoreline change at that location.

3.2.3. Sediment Transport

[34] Sediment transport for each shoreline cell is determined across its downdrift boundary using the angle determined as described above (Figure 7). Breaking wave depth and height, computed by refracting deepwater waves onshore, are inserted into (1) to determine Q_s across the boundary. Multiplying Q_s by the iteration time step, Δt, determines the volumetric quantity of sediment transported (m^3, deposited) from the selected cell.

[35] Although we have demonstrated that the deepwater reference frame aids the formal understanding of the shoreline instability, it is breaking waves that cause alongshore sediment transport. Therefore, although deepwater wave characteristics are input in the model, the algorithm uses (1) and breaking wave quantities determined from refraction and shoaling over shore-parallel contours to compute Q_s. Using (1) makes this model more similar to traditional one-line models, and accounts for factors such as the case where breaking waves are not fully shallow water. Also, if more complex wave refraction were treated, the computed wave heights and angles could just as easily be inserted into (1).

3.2.4. Shoreline Adjustment

[36] The fractional value of each shoreline cell is updated using the difference between influxes (Q_{in}) and outfluxes (Q_{out}), divided by its plan view area and contributing shoreface depth (including the subaerial berm height, B (Figure 2)):

$$\Delta F = \frac{(Q_{in} - Q_{out})}{(D_{sf} + B)\Delta W^2}. \tag{9}$$

[37] On open ocean coasts, shorefaces extend on the order of a kilometer, and we use cell sizes of 100 m. Lacustrine, back barrier, or other low wave energy environments could be simulated with a smaller representative cell size.

[38] Simulations presented here use periodic lateral boundary conditions: sediment passing off the right domain edge returns on the left side and vice versa. Initial conditions consist of a straight beach with white noise perturbations (maximum magnitude one cell width) to the shoreline at each alongshore cell.

3.2.5. Shoreface Depth

[39] The shoreface depth, D_{sf}, is determined by finding the intersection of a shoreface, sloping perpendicular (S_{sf}, 0.01 in all simulations) to the shoreline orientation, with a continental shelf sloping away (S_{cs}, 0.001 in all simulations) from the regional shoreline orientation. As a shoreline accretes across the continental shelf, it faces increasing shoreface depths, and the shore will accrete less for a given convergence of alongshore sediment flux. Eroding shore-
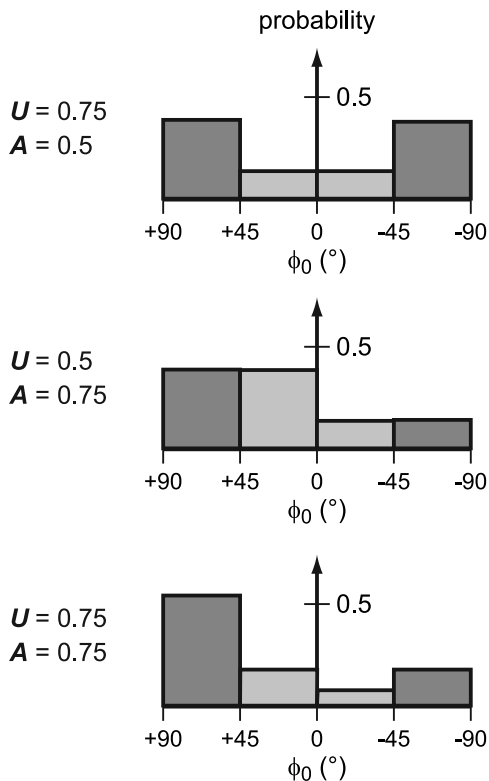
Figure 8. Sample wave climate probability distribution functions, where U represents the fraction of unstable, high-angle waves and A represents the fraction of waves approaching from the left, looking offshore ($\phi_0 > 0$).

lines remove sediment to a minimum shoreface depth, D_{min}, representing an effective wave base (10 m in all simulations) (Figure 2).

[40] This phenomenon of accreting to increasing depths and eroding to a fixed depth could lead to a hysteresis where mass is left behind if a shoreline accretes then subsequently erodes. Therefore the model algorithm also tracks whether or not a shoreface has accreted past a given cell, although this detail does not alter the basic simulation results.

3.2.6. Barrier Overwash
[41] As spits extend offshore due to the high wave angle instability, erosion on the updrift flank thins the spit. Although this thinning can result in spit "breaching", in nature barriers tend to be sustained by the process of barrier overwash, maintaining a minimum width [*Leatherman*, 1979]. We have added a schematized process of barrier overwash, transporting sediment from the front to the back of a sufficiently narrow barrier, to the basic model. We implement a novel analytical solution that extends upon this concept of a minimum barrier width [*Leatherman*, 1979] and its implementation in a numerical model by *Jiménez and Sánchez-Arcilla* [1999, 2004] (see Appendix A).

3.3. Input Wave Climates
[42] The model simulations presented here involve approach angles selected from a probability distribution function (PDF) controlled by two variables. The fraction of waves approaching from high versus low angles, or the proportion of unstable waves, is controlled by U. The other variable, the wave climate "asymmetry", A, determines the fraction of waves approaching from the left relative to the regional shoreline trend (i.e., the fraction of waves that will result in alongshore sediment transport to the right facing offshore) (Figure 8). After a specified duration (typically a simulated day), a new wave approach angle is selected according to the PDF.

[43] These two variables, U and A, represent the "parameter space" explored here. Other wave variables, such as height and period, are held constant in and across all simulations shown here ($H_0 = 2$m, $T = 8$ s, representing a passive margin, open ocean coast such as the U.S. east coast). These wave variables held constant do not affect the instability or subsequent model behaviors; rather, they affect the time scaling of the simulations (see section 5).

[44] Wave angle PDFs can be related to wave climates measured in nature [*Ashton and Murray*, 2006], with the probability in each angle bin (with bins typically narrower than in Figure 8) representing the cumulative contributions to alongshore sediment transport from waves from a given direction. Large wave events in nature translate to more frequent waves from that angle in the constant wave height model. However, seasonal shifts or storms can result in temporal correlation in the alongshore sediment transport caused by waves in the same directions. The random schematization of wave approach angles in the model overlooks these effects by spreading concentrated wave energy events over time.

4. Model Results and Predictions

[45] In all simulations with wave climates predominated by high-angle waves ($U > 0.5$), undulations arise from the initially straight, slightly perturbed shoreline. At first, these bumps have small wavelengths, on the scale of the model grid resolution. Finite amplitude interactions soon dominate shoreline evolution, and these undulations continue to grow and interact, increasing in wavelength and aspect ratio. Whenever the input wave climate is asymmetric, with more waves approaching from one alongshore direction than another ($A \gtrless 0$), the growing features translate in the direction of net sediment transport.

4.1. Modes of Coastal Evolution
[46] Simulations suggest five basic types of shoreline response as the wave climate variables U and A are varied (Figure 9; also see animations in the auxiliary material)[1]. The first mode is the simplest: whenever more low-angle than high-angle waves approach the shore ($U < 0.5$), the shoreline flattens (not shown). We have classified the other, more interesting behaviors for high-angle wave climates into four general categories: migrating alongshore sand waves, cuspate bumps, flying spits, and reconnecting spits (Figure 9). Although Figure 9 showcases the end-members of this classification scheme, there exists a continuum between these responses.

4.1.1. Alongshore Sand Waves
[47] For climates with a slight predomination of high-angle waves and a moderate amount of directional asymmetry, simulated bumps translate in the direction of net

---
[1]Auxiliary materials are available in the HTML. doi:10.1029/2005JF000422.

transport, increasing in size over time (Figure 9b). High-angle waves from the dominant transport direction cause erosion on a bump's updrift flank. Beyond this inflection point, high-angle waves deposit sediment, driving the updrift inflection point toward the bump's crest (Figure 5). Much of this deposition occurs downdrift of the crest, with low-angle waves in the distribution spreading it farther downdrift. These alongshore sand waves grow over time by merging; when one migrating feature overtakes another, the two features join, creating a larger sand wave.

[48] If the cross-shore/alongshore aspect ratio of the features is significant, "shadow zones" extend from each bump, trapping all the sediment transported past its crest. Gross alongshore sediment transport therefore imposes an upper limit on downdrift migration rates. Both small and large features can trap sediment in their shadow zones at the same rate. However, for the same amount of trapped sediment, a smaller sand wave will translate further downdrift than a larger sand wave; migration rates scale inversely with the plan view area of the feature. Therefore smaller sand waves translate downdrift faster than larger ones, eventually overtaking the larger features and merging with them. This behavior is similar to that of simulated aeolian ripples, which is not entirely surprising as a fundamentally similar angle-based instability initiates the evolution of both systems [*Anderson*, 1990].

[49] A shadow zone also tends to starve the updrift flank of the next sand wave of alongshore sediment flux, resulting in a sediment deficit and subsequent erosion. Occasionally, the erosion downdrift of small sand waves migrating up the flank of a larger sand wave "repels" the tip of the larger sand wave, shedding a new, even smaller sand wave before the first two sand waves merge. Typically, this new sand wave migrates quickly due to its particularly small size, soon merging with the next updrift feature. This repelling behavior, also seen in models of aeolian ripples [*Werner and Kocurek*, 1998; *Prigozhin*, 1999], demonstrates how features can interact over long ranges.

4.1.2. Cuspate Bumps

[50] When there is little to no asymmetry in the wave climate, features still interact and grow, but do so through an entirely different mechanism. Without a strong asymmetry to the wave climate, features extend in the cross-shore direction faster than they translate alongshore, and do not merge by overtaking one another. Instead, as these "cuspate bumps", extend offshore, they interact by influencing each other's local wave climates through wave shadowing (Figures 9c and 9d).

[51] As cuspate bumps emerge, slightly larger shapes grow faster than, and at the expense of, their smaller neighbors by outcompeting them for high-angle waves. As a larger bump extends offshore, its tip will experience a relatively large proportion of high-angle waves while shadowing smaller neighboring bumps from many of the highest-angle waves. Eventually, as a larger bump grows, robbing a smaller neighbor of more and more high-angle waves, it does not just outcompete its neighbor for high-angle waves, the smaller bump's wave climate eventually becomes predominated by low-angles waves and it diffuses away. As these smaller bumps disappear, their mass is added to the neighboring larger bumps, further reinforcing the positive feedback feeding the larger bumps.

[52] Simulations show the development of a series of cuspate bumps of roughly similar spacing and height whenever wave climates are relatively symmetric (Figure 9a). As U is increased, these features increase their cross-shore extent and become more cuspate, changing from sinusoidal undulations (Figure 9c) to more pointed features (Figure 9d). This increased aspect ratio for higher-angle wave climates arises due to the eventual development of a quasi-steady state in which the transport of sediment toward the cape tips by high-angle waves is approximately counterbalanced by low-angle waves sweeping sediment back toward the embayments. For wave climates with larger proportions of high-angle waves, steeper flanks are required to increase the effectiveness of the low-angle waves transporting sediment toward the embayments.

[53] With slight wave climate asymmetries, these features migrate in the direction of net alongshore transport, but do so slowly, and no not "overtake" one another as the alongshore sand waves do. Slight wave climate asymmetries can also increase the "pointiness" of the cape tips.

[54] As bumps grow, the local wave climates along their flanks change because of both wave shadowing and the change in the shoreline orientation itself. A rotated shoreline feels a different proportion of high- and low-angle waves than one with the global average orientation. Ultimately, the local wave climates along the flanks become predominantly low-angle (a phenomenon explored in further detail by *Ashton and Murray* [2006]). These locally low-angle waves explain why new, small bumps do not continue to form along the flanks of larger bumps: A little bump superimposed upon a larger one will feel a different wave climate than the large bump itself.

4.1.3. Spits

[55] For more asymmetrical wave climates, spits begin to extend off of the ends of growing cuspate bumps (Figure 9e). These seaward extending "flying spits" evolve in a manner similar to that predicted for a single shape influenced by waves from a single high angle (Figure 5). Once formed, spits continue to extend seaward due to sediment deposition in shadow zones behind the spit tip. This shadow zone traps all of the sediment that enters, which tends to be a significant quantity as flying spits only occur in strongly asymmetrical wave climates (Figure 9a). Because the spits themselves represent relatively small quantities of sand, and they extend at rates determined by gross alongshore sediment transport, spits extend offshore at rates much faster than the migration rate for cuspate bumps.

[56] Spits also interact and eliminate one anther, increasing in cross-shore extent and wavelength over time. Rapid spit extension tends to block downdrift neighbors from the dominant waves. Within the protected lee of the flying spits, waves are effectively blocked from both the dominant high-angle direction and from all low angles. Consequently, wave climates in the lee are typically dominated by high-angle waves approaching from a direction opposite to that of the net alongshore drift. This leads to the formation of "reverse" flying spits off of both the mainland coasts and on the landward face of the main spit. Sometimes, the reverse spits off of the mainland can fuse with the main spit, enclosing a lagoon (Figure 9e).
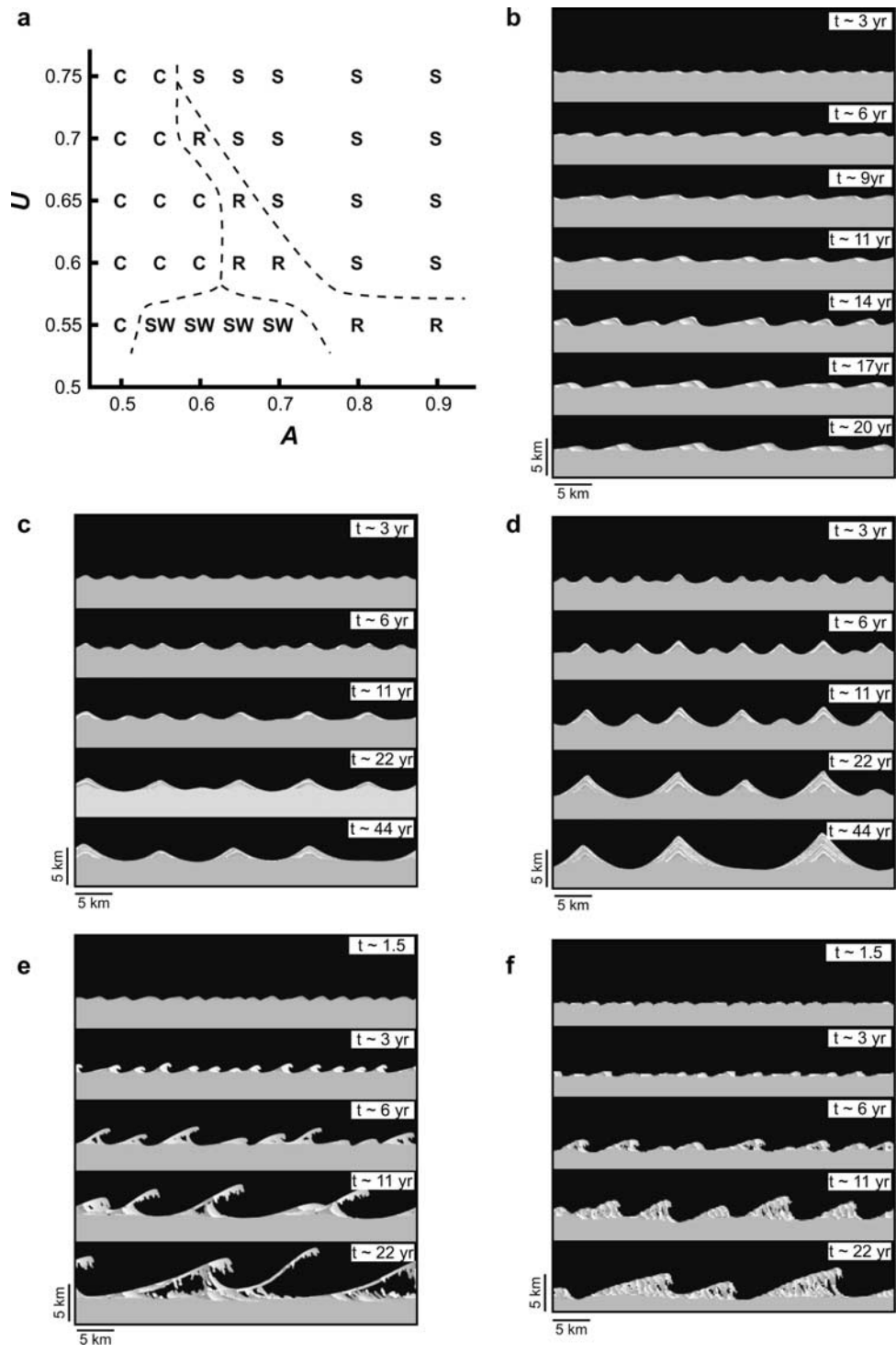
Figure 9. (a) Different modes of simulated shoreline response as U and A are varied. C represents cuspate bumps, SW represents alongshore sand waves, R represents reconnecting spits, and S indicates flying spits. Also shown are progressive stacks of the plan view model domain demonstrating typical simulation responses: (b) migrating alongshore sand waves (SW, $A = 0.65$, $U = 0.55$), (c) subtle cuspate bumps (C, $A = 0.5$, $U = 0.6$), (d) more pronounced cuspate bumps (C, $A = 0.5$, $U = 0.7$), (e) flying spits (S, $A = 0.7$, $U = 0.65$), and (f) reconnecting spits (R, $A = 0.7$, $U = 0.6$). Cells along the shoreline are plotted with a shading brightness proportional to the fractional amount of sediment within the cell. Sediment deposited contemporaneously is plotted with the same color. Animations of these simulations can are in the auxiliary material.
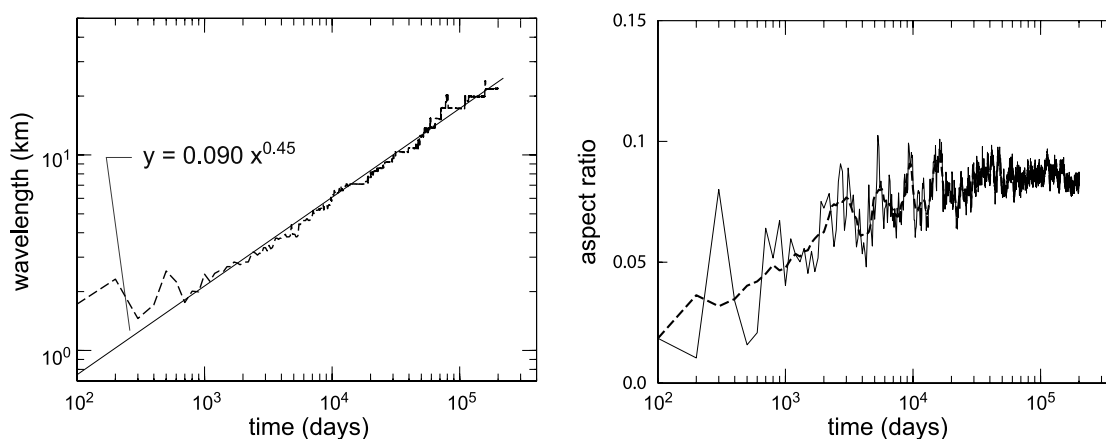
Figure 10. Wavelength and aspect ratio evolution for a simulation with $A = 0.5$ and $U = 0.6$, with a power law fit to the wavelength growth (dashed line) and an 11-point running average of the time series (solid line). Aspect ratio is defined as the peak to trough amplitude divided by the wavelength, and the simulated coast is 2500 cells wide, with $\Delta W = 100$ m and $\Delta t = 0.1$ day.

[57] Between the parameter space where cuspate bumps and full-fledged flying spits form, slightly different evolution occurs, generating features we have termed "reconnecting spits" (Figure 9f). As with flying spits, spit heads form off of the end of the initial cuspate bumps. However, the extension of these spit heads is short-lived, and either low-angle waves or high-angle waves from the subordinant direction flatten and redirect the spit tip, causing it to veer toward, and eventually reconnect with, the mainland.

4.2. Aspect Ratios and Wavelength Growth

[58] As discussed above, the initial growth of infinitesimal perturbations under high-angle waves is an antidiffusional process (has a negative diffusivity). However, shoreline features grow and self-organize due to emergent, long-range interactions unrelated to the initial instability. A quantitative examination shows that despite these complicated interactions, in most simulations perturbation wavelength grows at a rate roughly proportional to, but consistently slightly less than, the square root of time, approximating the analytically predicted diffusional timescale (Figure 10). Although wavelengths continue to grow, the features eventually attain a statistically constant aspect ratio (Figure 10).

[59] Cuspate bumps derived from a symmetrical wave climate with differing U all show approximately the same temporal scaling for wavelength growth despite differences in cross-shore/alongshore aspect ratios (Figures 9c, 9d, and 11a). These results suggest that, despite the stronger instability, increasing the proportion of high-angle waves does not significantly affect the rate that bumps merge.

[60] If the proportion of high-angle waves is held constant, increases to the wave asymmetry do not initially affect aspect ratios (Figure 11b), and the diffusional time scaling is maintained. However, when the asymmetry increases enough that spits begin to form (Figure 9a), aspect ratios increase dramatically, about twofold. Wavelength growth also appears to increase slightly when spits emerge. Comparisons of averaged results from simulations with a stronger predominance of high-angle waves more clearly illustrates both the aspect ratio increase and the temporary

quickening of wavelength growth (Figure 11c). Power laws fit to these results, however, suggest almost the same long-term temporal scaling.

4.3. Model Sensitivity

[61] Tests indicate that the model is insensitive to variations in the model-specific parameters. First, model results are independent of the types and magnitude of the initial perturbation. As long as model time steps remain within numerical stability limits, simulation results depend on neither the iteration time step nor upon the duration between changes in the angle of wave approach. Simulations addressing very large spatial and temporal scales can therefore use large time steps and change wave approach angles less frequently than once per simulated day.

[62] Model results are insensitive to spatial grid resolution; simulations with symmetrical wave climates but using different spatial resolution (ΔW) exhibit statistically equivalent wavelength and aspect resolution evolution. However, inclusion of barrier overwash introduces a spatial scale, placing places a maximum on ΔW, as mentioned above.

[63] Model sediment is conserved with a high degree of accuracy in simulations featuring moderate coastline curvatures. However, the one-line assumption that erosion/accretion occurs in a polyhedron with a rectangular plan view shape becomes less tenable where the coastline curvature is extreme, such as behind a flying spit or at a spit end. Mass conservation limits the range of wave climates and behaviors the model can meaningfully simulate, and results become increasingly unrealistic in the limit of large values of U and A. Alleviating this problem would require a model that explicitly tracks subaqueous bed elevations.

5. Discussion and Conclusions

5.1. Natural Shoreline Features

[64] The simulated high wave angle features resemble landforms found along many sedimentary coasts. What we have termed flying spits within the simulation results (Figure 9e) have also been called cuspate spits [*Fisher*, 1955; *Zenkovich*, 1959] and have even been referred to as a type of "zetaform" beach even when there is no rocky
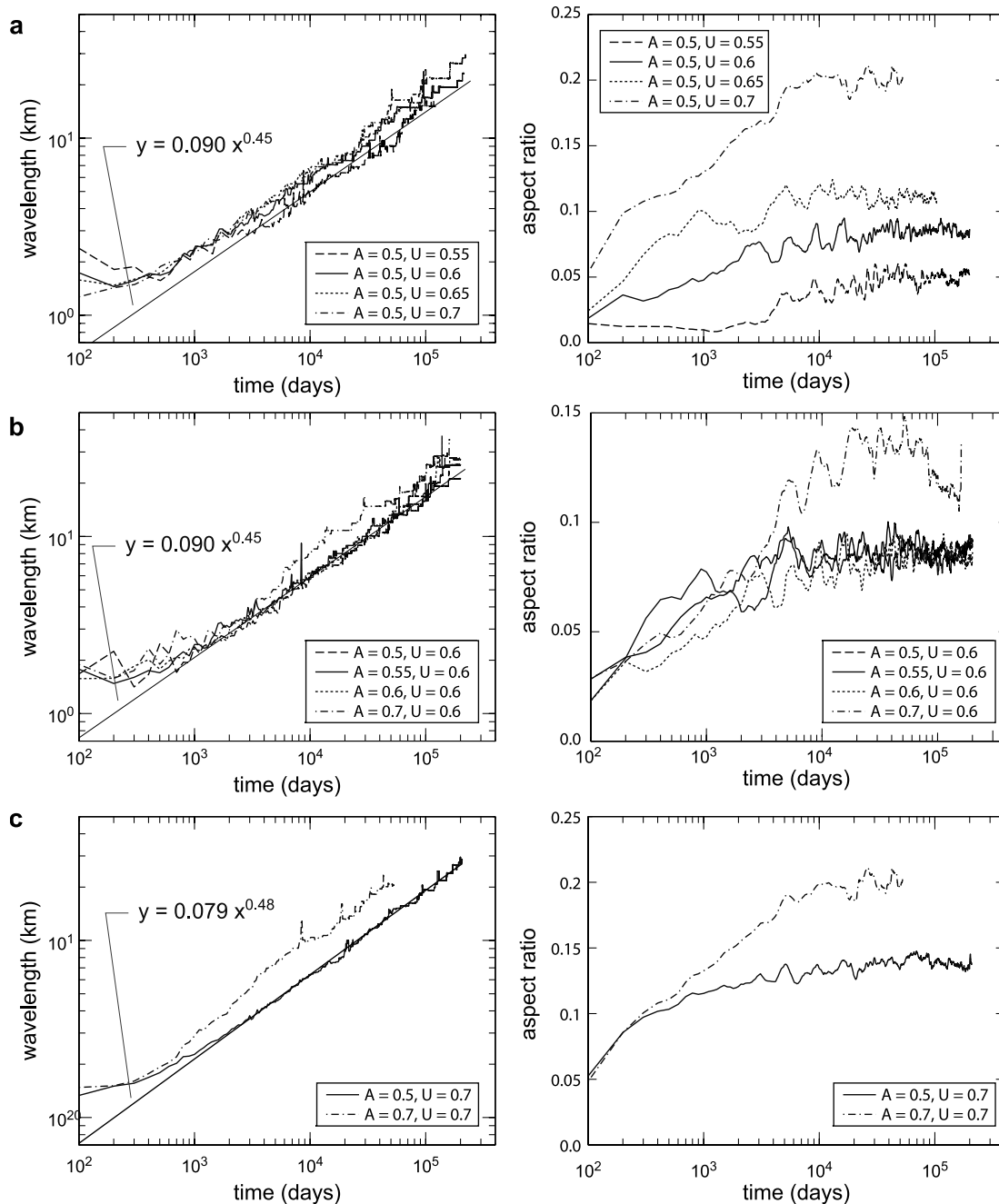
Figure 11. Plots of wavelength and aspect ratio (fit with an 11-point temporal running average for clarity, as demonstrated in Figure 10) changes over simulated time for (a) $A = 0.5$ with varying U (including a power law regression fit to $U = 0.6$), (b) $U = 0.6$ with varying A (including a power law regression fit to $A = 0.5$), and (c) averaged response of three simulations with $A = 0.5$ and $U = 0.7$ and three other simulations with $A = 0.7$ and $U = 0.7$.

headland control (such as the west coast of Sri Lanka) [*Davies*, 1980]. Examples of series of flying spits can be found along the Ukrainian coast of the Sea of Azov [*Zenkovich*, 1959; *Ashton et al.*, 2001], on the Namibian coast [*Elfrink et al.*, 2003] and along the eastern Russian coast [*Zenkovich*, 1967] (Figure 12a). Both the Azov Sea spits and the Namibian spits are affected strongly by waves approaching at high angles [*Ashton et al.*, 2001; *Elfrink et al.*, 2003], and the example presented here for the Russian coast (Figure 12a) is within a strait where ocean waves can only

approach from high angles. These features are also often found in enclosed lagoons where fetch limitations result in dominant high-angle wave approach [*Zenkovich*, 1959].

[65] Examples of cuspate bumps, or series of cuspate forelands, can be found along the Carolina coast of the southeastern United States. and in the back-barrier environment of Nantucket Harbor, United States (Figure 12b). The Carolina Capes are affected by northeastern waves from winter storms and southerly waves from tropical storms, both of which approach at high angles compared to the

shoreline trend [*Ashton et al.*, 2001]. *Rosen* [1975], following Zenkovich's concepts, demonstrates that within Nantucket Harbor, tidal fluctuations are low, and the greater fetch across the long axis of the harbor results in high-angle wave dominance.

[66] Migrating alongshore sand waves are found along many coasts. Sometimes these are visually obvious [*Stewart and Davidson-Arnott*, 1988; *Thevenot and Kraus*, 1995; *Davidson-Arnott and Van Heyningen*, 2003], or they may manifest themselves as migrating zones of erosion and accretion [*Bruun*, 1954; *Verhagen*, 1989; *Ruessink and Jeuken*, 2002]. Because sand waves occur in the model when high- and low-angle waves are almost balanced, correlating their appearance with high-angle waves requires more detailed techniques (as described by *Ashton and Murray* [2006; *Ashton et al.*, 2003]).

[67] Field investigations of alongshore sand waves suggest that these features are often initially formed at the updrift side of the sand wave field through welding of ebb shoals after periodic inlet openings [*Thevenot and Kraus*, 1995], through episodic sediment bypass [*Ruessink and Jeuken*, 2002], or through the welding of offshore bars [*Davidson-Arnott and Van Heyningen*, 2003]. Sand waves thus formed migrate downdrift, smaller ones traveling faster than larger ones, sometimes merging as one sand wave overtakes another [*Stewart and Davidson-Arnott*, 1988; *Thevenot and Kraus*, 1995]. Sand wave formation in the model superficially appears to be different, with the entire sand wave field forming simultaneously. However, because early model behavior arises from the arbitrarily defined initial conditions, the initial model evolution is less significant than the finite amplitude behaviors, such as the migration and merging of sand waves, that later emerge. If sand waves only tend to form at the updrift limit of a sand wave field, then both observations and simulations suggest that once such a field is formed, features are self-organized in a manner that inhibits the formation of new undulations within the sand wave field itself.

5.2. Rescaling Simulation Results

[68] The results presented in Figure 9 show relatively small features (~10 km) that evolve over geologically short timescales (<50 years). However, the diffusional time scaling upheld over many orders of magnitude (Figure 11) suggests that these results can be rescaled to generally apply to a different wave-dominated environment using (8):

$$\Delta t \propto \left(\frac{K_1}{D_{sf}} H_0^{\frac{12}{5}} T^{\frac{1}{5}} \right) \Delta x^2. \qquad (10)$$

[69] For example, Figures 9c and 9d shows that a shoreline develops 10 km wavelength cusps in approximately 50 years; (10) suggests that, other things being equal, a tenfold increase in wavelength should take a hundredfold longer to develop, or 100 km wavelength features should take on the order of 5000 years to form.

[70] The other relationships in (10), representing the proportionality between Δt and Δx^2, are intuitive: increasing the shoreface depth, D_{sf}, will slow coastal evolution, and increasing wave height (and period) and the sediment transport coefficient will speed up shoreline changes.

D_{sf} depends on H_0, T, and sediment characteristics [*Hallermeier*, 1981]; coasts with smaller, shorter period waves, and coarser sediment will have a smaller shoreface depth, and vice versa. The effective shoreface depth tends to increase as longer timescales are considered [*Stive et al.*, 1991]. Of the scaling factors, K_1 is the most poorly constrained, as this typically empirical coefficient can vary drastically between different sites [*Wang et al.*, 1998].

[71] These results suggest that a potential order-of-magnitude determination of the age of a cuspate coast created by high-angle wave could be made from the spacing of features. However, nature rarely starts from a straight initial configuration, and larger-scale initial morphodynamic perturbations could easily short-circuit this diffusional timescale. A more robust prediction from the model is that regardless of age, the aspect ratio of coastal features should be indicative of the proportion of high-angle waves. This prediction is insensitive to the type and amplitude of the initial perturbations.

[72] The diffusional scaling predicted in (10) suggests that time alone cannot prevent a set of cuspate features from continuing to grow and merge. This scaling, however, only applies while the underlying model assumptions remain appropriate. In nature, as capes or other features increase in size, other processes may increase in importance, slowing or even stopping cape growth and merging. For instance, as capes become significantly large, the development of residual offshore tidal currents can lead to the sedimentation and extension of shoals offshore of cape tips [*McNinch and Wells*, 1999; *McNinch and Luettich*, 2000]. As features get larger, wave generation within the cape embayments exerts a stronger influence, and alongshore variations in local wind waves play an increasing role, with meteorological conditions determining whether locally generated waves provide a negative or positive effect on cape evolution.

5.3. Discussion

[73] Our model evolves the shoreline only due to gradients in alongshore sediment transport, and does not account for relative sea level, which changes over these same geologic timescales that would be required for some large-scale features to develop. However, even small gradients in alongshore sediment flux easily overwhelm rates of cross-shore transport due to sea level changes [*Cowell et al.*, 1995]; a general landward shoreline retreat maintaining a defined shoreface during sea level rise could be superimposed without greatly altering the results shown here. During lowstands, abandoned cuspate shorelines [*Moslow and Heron*, 1981] may remain until sea level rises again, affecting subsequent shoreline development, possibly "jumpstarting" the evolution of cuspate coasts. Model results show that, even on geologic timescales, regression and transgression could occur simultaneously along different portions of a cuspate coast even in the absence of a sediment source or along-coast differences in rates of sea level change.

[74] The model also assumes that the entire shoreface is composed of mobile, sandy sediment. Even along a passive margin like the east coast of the United States, rock and consolidated mud outcrop in the shoreface [*Riggs*, 1995]. However, as long as shoreface weathering can maintain a veneer of mobile, noncohesive sediment, a coast can still be considered "sandy". Recent numerical experiments also
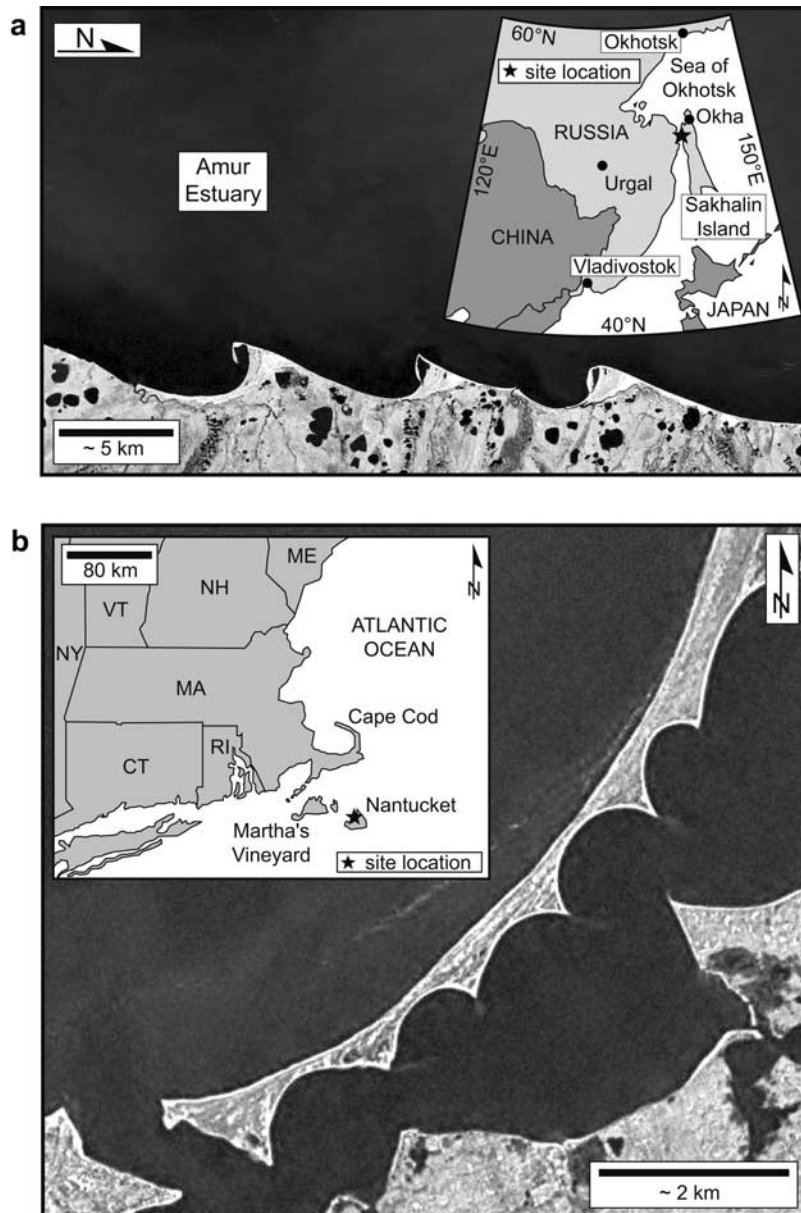
Figure 12. Natural examples of cuspate shorelines at (a) the eastern Russian coast in Amur Estuary and (b) Nantucket Harbor, Massachusetts. Data are available from USGS/EROS, Sioux Falls, South Dakota; source for this data set was the Global Land Cover Facility (http://www.landcover.org).

demonstrate that alongshore sediment transport tends to even out the effects of lithologic heterogeneities, potentially explaining the regional smoothness of even sediment-poor coastlines [*Valvo et al.*, 2006].

[75] Although the numerical model was not designed to represent or predict the time evolution of any one specific coast, it makes several important predictions regarding coastal evolution under the influence of high-angle waves. The key prediction is that whenever large-scale cuspate coastal features appear in a wave-dominated sedimentary environment, high-angle climates should be found. Therefore these features will often occur where a coastline changes orientation, where fetch limitations control wave approach angles, or at locations where meteorological conditions simply result in a predominance of high-angle

waves. The instability and the model predict not just the formation of these features, but diagnostic behaviors, such as the downdrift translation of high wave angle features due to finite-amplitude effects and how aspect ratios change with input wave characteristics. Migration is not predicted by the traditional one-line diffusion solution of *Pelnard-Consideré* [1956], although some studies have added an arbitrary advection term to the one-line diffusion solution [*Inman*, 1987; *Thevenot and Kraus*, 1995].

[76] Recent research by *Falqués and Calvete* [2005] expands upon the basic instability studied here using a more detailed linear stability analysis [*Murray and Ashton*, 2003]. This research, which includes the effects of wave refraction over bathymetry and a secondary competing term in the sediment transport formulation [*Ozasa and*

Brampton, 1980], does predict migration of infinitesimal amplitude features without the addition of arbitrary terms. More importantly, *Falqués and Calvete* [2005] suggest that the instability is damped as wave period increases and alongshore scales of perturbations decrease. As a result, the critical wave approach angle above which the instability occurs increases with decreasing alongshore scales and increasing wave periods. This reduction of the instability appears to be dependent on the shape of the offshore profile, while the influence of the additional, less common, Ozasa and Brampton sediment transport term remains unclear. In general, *Falqués and Calvete*'s [2005] research applies to the growth of infinitesimally small perturbations from an initially uniform state, and not necessarily to the finite amplitude, large-scale behavior that we predominantly focus on.

[77] The model simulates coastal evolution by computing sediment fluxes, using mass conservation to evolve the coast location. The eventual shape of the coast can change dramatically from the initial state, with coastal evolution and eventual form having little relation to the initial behavior (Figure 9). Previous researchers have associated rhythmic coastal features with edge waves [*Guza and Inman*, 1975; *Holman and Bowen*, 1982]. Although these infragravity edge waves are usually associated with features occurring at spatial scales smaller than 1 km, some researchers, such as *Dolan et al.* [1979] and *Sánchez et al.* [2003], have suggested a link between large-scale cuspate features and standing edge waves. Unlike these approaches that focus on hydrodynamic templates without investigating feedbacks with sediment transport processes, our approach focuses on physical processes and the feedbacks between the evolving coast and sediment transport, allowing for alteration and migration of features after their initial formation. The hypothesis that alongshore sediment transport alone can result in the formation through self-organization of large-scale (kilometers to hundreds of kilometers on an open ocean coast) quasi-rhythmic features differs substantially from previous hypotheses that used hydrodynamic templates or geological inheritance to set the wavelength of these large-scale cuspate features.

[78] We have been surprised by some of the rich behaviors that emerged from the simple interactions built into the model. Some of the key types of simulated behavior, such as wave shadowing interactions for symmetrical wave climates and the shape and evolution of flying spits, were unexpected during model development, and the development of these features represents a model "prediction". Although these emergent forms of behavior, and their occurrence in nature [*Ashton and Murray*, 2006], can be understood after they had been observed in the model, the model has in no way been "calibrated" or "tuned" to make these features appear. The only process added in response to initial model results is barrier overwash.

5.4. Summary

[79] Properly formulating coastal evolution in terms of deepwater wave quantities reveals a strong wave angle dependence of coastal evolution, resulting in an instability in the plan view shape of a coast. This sensitivity to wave angle has long been overlooked, mostly because nearshore refraction makes even the most oblique swells break at small angles. Simulations show that high-angle waves could be responsible for the self-organization of large-scale coastal shapes such as flying spits and cuspate bumps to more subtle alongshore sand waves that may only manifest themselves as measured zones of accretion and erosion. Wave climate details, particularly the proportion of high-angle waves and the directional distribution of approaching waves, determine the types of shapes that evolve due to the instability. The proportion of high-angle waves also controls the aspect ratio of shoreline features, a phenomenon further investigated by examining wave climate statistics by *Ashton and Murray* [2006].

Appendix A: Barrier Overwash Formulation and Implementation

A1. Overwash Formulation

[80] Thinning of barriers promotes front-to-back transport by increasing the likelihood of wave overtopping and temporary inlet formation during storms [*Leatherman*, 1979; 1983]. Although some wider barriers may be currently eroding along both landward and seaward shores due to sea level rise [*Leatherman*, 1983], thin barriers such as Assateague Island, Maryland, (which is eroding due to local gradients in alongshore sediment transport) tend to maintain a constant critical width [*Leatherman*, 1979]. Here we present an analytical solution for the maintenance of a minimum barrier width by overwash, extending upon the iterative implementation of this concept in a numerical model by *Jiménez and Sánchez-Arcilla* [1999, 2004].

[81] The high wave angle instability leads to offshore extension of spits with erosional updrift flanks (Figure 5). Eventually, this can thin the offshore-extending spit until it is "breached", which leads to, amongst other problems, computational difficulties when the spits become detached from the mainland shoreline. In nature, overwash tends to elevate barriers, and if the depth of back-barrier deposition is less than the shoreface depth, overwash will also widen barriers. Our approach assumes that overwash will occur frequently until low areas are filled with sediment and a barrier achieves a minimum height, equal to the berm height, B, [*Cowell et al.*, 1995] and until the barrier widens to a critical width, W_e, [*Leatherman*, 1979; *Jiménez and Sánchez-Arcilla*, 1999]. This approach assumes that even if overwash events contribute to short-term breaches, they will not result in permanent inlets. The underlying assumptions are therefore more appropriate for long-term evolution and locations with small tidal ranges relative to the wave energy.

[82] If overwashed sediment is conserved, the depth of back-barrier sediment accumulation, D_{bb}, and the erosional shoreface depth, D_{sf}, control the ratio of the width of back-barrier accumulation, ΔY_{bb}, to the width of shoreline erosion, ΔY_{sl}:

$$\Delta Y_{bb} = \frac{(D_{sf} + B)}{(D_{bb} + B)} \Delta Y_{sl} \qquad (A1)$$

(Figure A1). This equation can be solved iteratively [e.g., *Jiménez and Sánchez-Arcilla*, 2004], or analytically for a
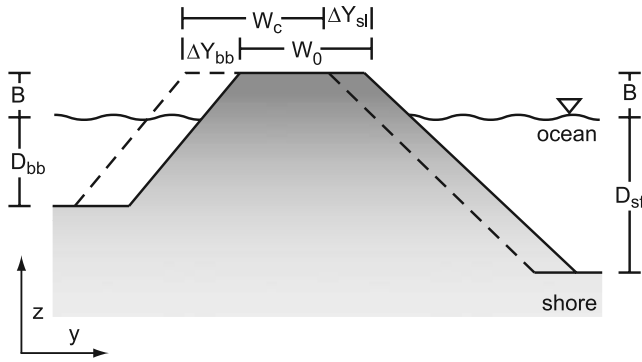
Figure A1. Schematic cross section of mass-conserving barrier overwash enforcing a critical barrier width, W_e. Contributions from the shoreface result in barrier widening if $D_{sf} > D_{bb}$. Within the numerical model, $D_{sf} = D_{min}$ during overwash.

given barrier width (W_0) deficit ($W_0 < W_e$) using the relationship:

$$W_c = W_o + \Delta Y_{bb} - \Delta Y_{sl}. \tag{A2}$$

[83] Combining (A1) and (A2) yields

$$\Delta Y_{bb} = \frac{(W_c - W_0)}{\left(1 - \frac{(D_{bb} + B)}{(D_{sf} + B)}\right)} \tag{A3}$$

and

$$\Delta Y_{sl} = \frac{(W_c - W_0)}{\left(\frac{(D_{sf} + B)}{(D_{bb} + B)} - 1\right)} \tag{A4}$$

[84] The critical height and width concepts could be extended to model barrier response to changes in relative sea level. However, the one-line model described here does not account for changes in sea level, and this exercise remains beyond the scope of this investigation.

A2. Model Implementation

[85] At each time step, the model checks the local barrier width at each shoreline cell, measured in a direction perpendicular to the cell-centered shoreline angle. If the barrier is narrower than W_e, overwash occurs, updating the shoreline and back-barrier positions according to (A3) and (A4). To buffer discretization artifacts, we impose a maximum ΔY_{bb} of 0.2 cell widths per time step. As suggested by *Leatherman* [1979], we use W_e of 250 m, representative of an open ocean, wave-dominated coast such as the eastern coast of the United States. The model algorithm requires that barriers be a minimum of several cells in width; ΔW must be less than W_e.

[86] Knowledge about back-barrier depths (D_{bb}) is required to compute overwash into a back-barrier region created by the seaward extension of a cuspate spit. The model algorithm tackles this problem by taking a simplified approach, assuming that shorefaces of similar slopes extend from the coast in all directions, including the back barrier and the backing mainland coast. Correspondingly, D_{bb} is computed as the depth of the intersection of shorefaces extending from the back barrier and from the backing shoreline. While inexact, this "rule" for back-barrier depth captures the basic geometric principal that back-barrier depths should be shallower closer to the mainland shoreline. Spits realize diminishing benefits from overwash as they extend offshore. More exact computation of back-barrier depths would require keeping track of bed elevations across the domain, a considerable departure from the one-line approach.
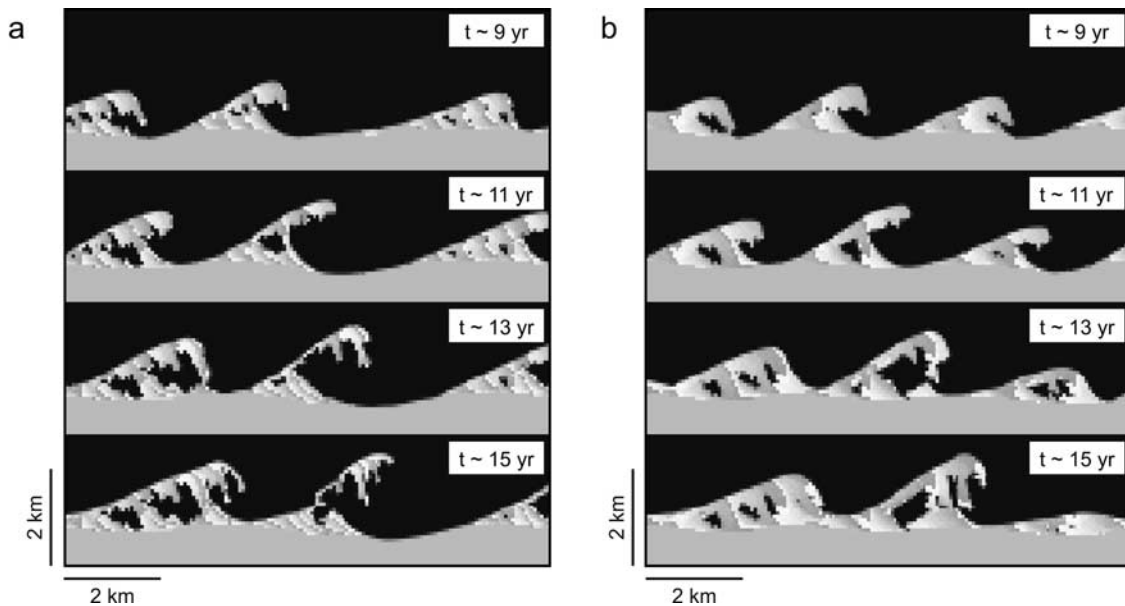

Figure A2. Plan view time stacks of flying spits for simulations (a) without and (b) with barrier overwash ($A = 0.7$, $U = 0.65$). Without overwash, spit "necks" break, and simulated spits disconnect from the mainland.

[87] Spit breaching can be seen in simulations without overwash, where erosion eventually disconnects the spits from the mainland (Figure A2a). Overwash extends simulations by allowing spits to maintain a nearly uniform width (Figure A2b).

References

Anderson, R. (1990), Eolian ripples as examples of self-organization in geomorphological systems, *Earth Sci. Rev.*, 28, 77–96.

Ashton, A., and A. B. Murray (2003), Self-organized behavior of modeled shoreline shapes, *Geophys. Res. Abstracts*, 5, Abstract 07703.

Ashton, A., and A. B. Murray (2006), High-angle wave instability and emergent shoreline shapes: 2. Wave climate analysis and comparisons to nature, *J. Geophys. Res.*, 111, F04012, doi:10.1029/2005JF000423.

Ashton, A., A. B. Murray, and O. Arnoult (2001), Formation of coastline features by large-scale instabilities induced by high-angle waves, *Nature*, 414, 296–300.

Ashton, A. D., A. B. Murray, and B. G. Ruessink (2003), Initial tests of a possible explanation for alongshore sandwaves on the Dutch coast, in *3rd IAHR Symposium on River, Coastal and Estuarine Morphodynamics*, pp. 310–319, Int. Assoc. of Hydraul. Res., Madrid.

Bakker, W. T. (1968), A mathematical theory about sandwaves and its applications on the Dutch Wadden Isle of Vlieland, *Shore Beach*, 36, 4–14.

Bruun, P. (1954), Migrating sand waves or sand humps, with special reference to investigations carried out on the Danish North Sea coast, *Proc. Coastal Eng. Conf., 5th*, 269–295.

Coco, G., D. A. Huntley, and T. J. O'Hare (2000), Investigation of a self-organization model for beach cusp formation and development, *J. Geophys. Res.*, 105, 21,991–22,002.

Cowell, P. J., P. S. Roy, and R. A. Jones (1995), Simulation of large-scale coastal change using a morphological behavior model, *Mar. Geol.*, 126, 45–61.

Davidson-Arnott, R. G. D., and A. G. Van Heyningen (2003), Migration and sedimentology of longshore sandwaves, Long Point, Lake Erie, Canada, *Sedimentology*, 50, 1123–1137.

Davies, J. L. (1980), *Geographical Variation in Coastal Development*, 2nd ed., Longman, New York.

Dean, R. G., and R. A. Dalrymple (2002), *Coastal Processes with Engineering Applications*, Cambridge Univ. Press, New York.

Deigaard, R., N. Dronen, J. Fredsoe, J. H. Jensen, and M. P. Jorgensen (1999), A morphological stability analysis for a long straight barred coast, *Coastal Eng.*, 36, 171–195.

de Vriend, H. J., M. Capobianco, T. Chesher, H. E. de Swart, B. Latteus, and M. J. F. Stive (1993), Approaches to long-term modelling of coastal morphology: A review, *Coastal Eng.*, 21, 225–267.

Dolan, R., and J. C. Ferm (1968), Crescentic landforms along the Atlantic Coast of the United States, *Science*, 159, 627–629.

Dolan, R., B. Hayden, and W. Felder (1979), Shoreline periodicities and edge waves, *J. Geol.*, 87, 175–185.

Elfrink, B., G. Prestedge, C. B. M. Rocha, and J. Juhl (2003), Shoreline evolution due to highly oblique incident waves at Walvis Bay, Namibia, in *Proceedings of the International Conference on Coastal Sediments 2003* [CD-ROM], World Sci., Hackensack, N. J.

Falqués, A. (2003), On the diffusivity in coastline dynamics, *Geophys. Res. Lett.*, 30(21), 2119, doi:10.1029/2003GL017760.

Falqués, A., and D. Calvete (2005), Large-scale dynamics of sandy coastlines: Diffusivity and instability, *J. Geophys. Res.*, 110, C03007, doi:10.1029/2004JC002587.

Falqués, A., G. Coco, and D. A. Huntley (2000), A mechanism for the generation of wave-driven rhythmic patterns in the surf zone, *J. Geophys. Res.*, 105, 24,071–24,087.

Fisher, R. L. (1955), Cuspate spits of Saint Lawrence Island, Alaska, *J. Geol.*, 63, 133–142.

Grijm, W. (1960), Theoretical forms of shorelines, *Proc. Coastal Eng. Conf., 7th*, 197–202.

Grijm, W. (1964), Theoretical forms of shorelines, *Proc. Coastal Eng. Conf., 9th*, 219–235.

Guza, R. T., and D. L. Inman (1975), Edge waves and beach cusps, *J. Geophys. Res.*, 80, 2997–3012.

Hallermeier, R. J. (1981), A profile zonation for seasonal sand beaches from wave climate, *Coastal Eng.*, 4, 253–277.

Hanson, H., and N. C. Kraus (1989), GENESIS: Generalized model for simulating shoreline change, report 1, Technical reference, U.S. Army Eng. Waterw. Exp. Stn., Coastal Eng. Res. Cent, Vicksburg, Miss.

Holman, R. A., and A. J. Bowen (1982), Bars, bumps, and holes: Models for the generation of complex beach topography, *J. Geophys. Res.*, 87, 457–468.

Hoyt, J. H., and V. J. Henry (1971), Origin of capes and shoals along the southeastern coast of the United States., *Geol. Soc. Am. Bull.*, 82, 59–66.

Inman, D. L. (1987), Accretion and erosion waves on beaches, *Shore Beach*, 55, 61–66.

Jiménez, J. A., and A. Sánchez-Arcilla (1999), Modelling of barrier-spit system evolution at decadal scale, in *Coastal Sediments '99*, pp. 1724–1738, Am. Soc. of Civ. Eng., Reston, Va.

Jiménez, J., and A. Sánchez-Arcilla (2004), A long-term (decadal scale) evolution model for microtidal barrier systems, *Coastal Eng.*, 51, 749–764.

Komar, P. D. (1971), The mechanics of sand transport on beaches, *J. Geophys. Res.*, 76, 713–721.

Komar, P. D. (1973), Computer models of delta growth due to sediment input from rivers and longshore transport, *Geol. Soc. Am. Bull.*, 84, 2217–2226.

Komar, P. D. (1983), Rhythmic shoreline features and their origins, in *Mega-Geomorphology*, edited by R. Gardner and H. Scoging, pp. 92–112, Clarendon Press, Oxford, U. K.

Komar, P. D. (1998), *Beach Processes and Sedimentation*, 2nd ed., 544 pp., Simon and Schuster, Upper Saddle River, N. J.

Larson, M., H. Hanson, and N. C. Kraus (1987), Analytical solutions of the one-line model of shoreline change, *Tech. Rep. CERC-87-15*, U.S. Army Waterw. Exp. Stn., Vicksburg, Miss.

Larson, M., H. Hanson, and N. C. Kraus (1997), Analytical solutions of one-line model for shoreline change near coastal structures, *J. Waterw. Port Coastal Ocean Eng.*, 123, 180–191.

Leatherman, S. P. (1979), Migration of Assateague Island, Maryland, by inlet and overwash processes, *Geology*, 104–107.

Leatherman, S. P. (1983), Barrier dynamics and landward migration with Holocene sea-level rise, *Nature*, 301, 415–417.

LeMehaute, E. M., and M. Soldate (1977), Mathematical modeling of shoreline evolution, *Proc. Coastal Eng. Conf., 16th*, 1163–1179.

List, J. H., and A. S. Farris (1999), Large-scale shoreline response to storms and fair weather, in *Coastal Sediments '99*, pp. 1324–1338, Am. Soc. of Civ. Eng., Reston, Va.

Longuet-Higgins, M. S. (1970), Longshore currents generated by obliquely incident waves, 1, *J. Geophys. Res.*, 75, 6778–6789.

Longuet-Higgins, M. S. (1972), Recent progress in the study of longshore currents, in *Waves on Beaches and Resulting Sediment Transport*, pp. 373–400, Elsevier, New York.

McNinch, J. E., and R. A. Luettich (2000), Physical processes around a cuspate foreland headland: Implications to the evolution and long-term maintenance of a cape-associated shoal, *Cont. Shelf Res.*, 20, 2367–2389.

McNinch, J., and J. T. Wells (1999), Sedimentary processes and depositional history of a cape-associated shoal, Cape Lookout, North Carolina, *Mar. Geol.*, 158, 233–252.

Moslow, T. F., and S. D. Heron (1981), Holocene depositional history of a microtidal cuspate foreland cape: Cape Lookout, North Carolina, *Mar. Geol.*, 41, 251–270.

Murray, A. B. (2003), Contrasting the goals, strategies, and predictions associated with simplified numerical models and detailed simulations, in *Prediction in Geomorphology, Geophys. Monogr. Ser.*, 135, edited by R. M. Iverson and P. R. Wilcock, pp. 151–165, AGU, Washington, D. C.

Murray, A. B., and A. Ashton (2003), Sandy coastline evolution as an example of pattern formation involving emergent structures and interactions, in *Proceedings of the International Conference on Coastal Sediments 2003* [CD-ROM], World Sci., Hackensack, N. J.

Murray, A. B., and A. Ashton (2004), Extending a 1-line modeling approach to explore emergent coastline behaviors, *Proc. Int. Conf. Coastal Eng., 29th*, 2035–2047.

Ozasa, H., and A. H. Brampton (1980), Mathematical modelling of beaches backed by seawalls, *Coastal Eng.*, 4, 47–63.

Pelnard-Consideré, R. (1956), Essai de teorie de l'evolution des formes de rivage en plages de sable et de galets, in *4th Journees de l'Hydraulique, Les Energies de la Mer, III*, pp. 289–298, La Houille Blanche, Grenoble, France.

Pelnard-Consideré, R. (1984), L'Hydraulique et la maıcirc;trise du littoral, paper presented at XVIII Journées de L'Hydraulique, Soc. Hydrotec. de Fr., Marseille, France.

Prigozhin, L. (1999), Nonlinear dynamics of aeolian sand ripples, *Phys. Rev. E*, 60, 729–733.

Riggs, S. R. (1995), Influence of inherited geologic framework on barrier shoreface morphology and dynamics, *Mar. Geol.*, *126*, 213–234.

Rosati, J. D., T. L. Walton, and K. Bodge (2002), Longshore sediment transport, in *Coastal Engineering Manual*, part II, *Coastal Sediment Processes*, edited by D. B. King, chap. III-2, U.S. Army Corps of Eng., Washington, D. C.

Rosen, P. S. (1975), Origin and progress of cuspate spit shorelines, *Estuarine Res.*, *2*, 77–92.

Ruessink, B. G., and M. C. J. L. Jeuken (2002), Dunefoot dynamics along the Dutch coast, *Earth Surf. Processes Landforms*, *27*, 1043–1056.

Sánchez, M. O., M. A. Losada, and A. Baquerizo (2003), On the development of large-scale cuspate features on a semi-reflective beach: Carchuna beach, southern Spain, *Mar. Geol.*, *198*, 209–223.

Stewart, C. J., and R. G. D. Davidson-Arnott (1988), Morphology, formation and migration of longshore sandwaves: Long Point, Lake Erie, Canada, *Mar. Geol.*, *81*, 63–77.

Stive, M. J. F., R. J. Nicholls, and H. J. deVriend (1991), Sea-level rise and shore nourishment: A discussion, *Coastal Eng.*, *16*, 147–163.

Thevenot, M. M., and N. C. Kraus (1995), Longshore sand waves at Southampton Beach, New York: Observation and numerical simulation of their movement, *Mar. Geol.*, *126*, 249–269.

Valvo, L. M., A. B. Murray, and A. D. Ashton (2006), How does underlying geology affect coastline change? An initial modeling investigation, *J. Geophys. Res.*, *111*, F02025, doi:10.1029/2005JF000340.

Verhagen, H. J. (1989), Sand waves along the Dutch Coast, *Coastal Eng.*, *13*, 129–147.

Walton, T. L., Jr., and R. G. Dean (1973), Application of littoral drift roses to coastal engineering problems, paper presented at First Australian Conference on Coastal Engineering, Natl. Comm. on Coastal and Ocean Eng., Inst. of Eng., Sydney, N. S. W., Australia.

Wang, J. D., and B. LeMehaute (1980), Criterion for stability of shoreline planform, *Proc. Coastal Eng. Conf., 17th*, 1295–1305.

Wang, P., N. C. Kraus, and R. A. Davis (1998), Total longshore sediment transport rate in the surf zone: Field measurements and empirical predictions, *J. Coastal Res.*, *14*, 269–282.

Werner, B. T., and T. M. Fink (1993), Beach cusps as self-organized patterns, *Science*, *260*, 968–971.

Werner, B. T., and G. Kocurek (1998), Bed-form dynamics: Does the tail wag the dog?, *Geology*, *25*, 771–774.

Wright, L. D., and A. D. Short (1984), Morphodynamic variability of surf zones and beaches: A synthesis, *Mar. Geo*, *56*, 93–118.

Zenkovich, V. P. (1959), On the genesis of cuspate spits along lagoon shores, *J. Geol.*, *67*, 269–277.

Zenkovich, V. P. (1967), *Processes of Coastal Development*, Oliver and Boyd, White Plains, N. Y.

————————————

A. D. Ashton, Department of Geology and Geophysics, Woods Hole Oceanographic Institution, MS 22, Woods Hole, MA 02543, USA. (aashton@whoi.edu)

A. B. Murray, Division of Earth and Ocean Sciences, Nicholas School of the Environment and Earth Sciences, Duke University, Durham, NC 27708, USA.